NEW METHODS TO DETECT PARTICLE VELOCITY AND MASS FLUX IN ARC-HEATED ABLATION/EROSION FACILITIES

D. B. Brayton, B. W. Bomar, B. L. Seiber, and P. D. Elrod
ARO, Inc., AEDC Division
A Sverdrup Corporation Company
Arnold Air Force Station, Tennessee 37389

ABSTRACT

Arc-heated flow facilities with injected particles are used at the Arnold Engineering Development Center (AEDC) to simulate the erosive and ablative/erosive environments encountered by spacecraft re-entry through fog, clouds, thermo-nuclear explosions, etc. Two newly developed particle diagnostic techniques used to calibrate these facilities are discussed. One technique measures particle velocity and is based on the detection of thermal radiation and/or chemiluminescense from the hot seed particles in a model ablation/erosion facility. The second technique measures a local particle rate, which is proportional to local particle mass flux, in a dust erosion facility by photodetecting and counting the interruptions of a focused laser beam by individual particles.

INTRODUCTION

Arc-heated particle-injected (seeded) flow facilities are used at Arnold Engineering Development Center (AEDC) to test nose cone materials and geometries by simulating the erosive and ablative/erosive environments of spacecraft re-entry. The two high-enthalpy, ablation testing (HEAT) facilities at AEDC each employ a seeded arc jet exiting into a low-expansion-ratio nozzle with relatively high static pressure (1 atm) to generate a high velocity (1500 $msec^{-1}$), high temperature (2000 to 4000°K), and high number density (a few particles per cm^3) dust cloud entrained in hot (2000 to 5000°K) gas that produces both erosion and ablation of models. The Dust Erosion Tunnel (DET) facility at AEDC employs a seeded arc jet exiting into a high-expansion-ratio nozzle with low static pressure (much less than 1 atmosphere) to generate a high velocity (1000 to 3000 $msec^{-1}$), low temperature (a few hundred °K), and low number density (1000 to 2000 per m^3) dust cloud entrained in a low-density, cool exitus gas that causes model erosion.

It is required that these facilities be calibrated regarding particle field characteristics. To this end two newly developed calibration instruments are described. One, the thermal emission velocimeter (TEV) measures the velocity of high-temperature particles in the HEAT facilities. Individual particle velocities are measured by collecting and photodetecting light self-radiated by a particle crossing two small, spatially separated, and separately photodetected regions in the flow. The two photodetected pulses then gate an electronic counter, thereby quantizing the time interval between pulses and providing the time versus distance measurement of velocity. Data is sequentially recorded, thereby providing a time-history of particle velocity at a point. The second instrument measures a local particle rate, which is proportional to local particle mass flux, in the DET facility by photodetecting interruptions or blockages of a laser beam as individual particles pass through the beam near its focus. Individual photodetected events are counted over fixed time intervals and recorded, thereby monitoring particle rate.

Measurements of both particle velocity and rate using these electro-optical techniques have been developed to the point that they are now effective, reliable diagnostic tools.

The remainder of this paper is concerned with the design and application of these instruments.

NOMENCLATURE

AEDC	Arnold Engineering Development Center
A_p	Cross-sectional area of particle; $\pi D_p^2/4$ for a spherical particle (m^2)
$\bar{A}_p$	Mean or average value of A_p (m^2)
ARO	Arnold Research Organization
ASA	American Standard speed (or exposure index) of a photographic emulsion (-)
A_v	Probe-volume virtual-aperture area or maximum cross-sectional area of the high detectivity region of the probe volume (m^2)
bit	Binary number (0 or 1) (-)
byte	Eight bits (-)
CRT	Cathode ray tube
DET	Dust Erosion Tunnel
D_f	Diameter of fiber optic (m)
D_ℓ	Diameter of lens or lens system aperture (m)
D_p	Diameter of particle (m)
D_v	Diameter of the probe-volume virtual aperture or diameter of the high-detectivity region of the probe volume (m)
Δf	Electronic bandwidth (Hz)
GPIB	General purpose interface bus
HEAT	High-enthalpy ablation testing
IEEE	Institute of Electrical and Electronic Engineers
k	Kilo or 1000
LV	Laser velocimeter
L_v	Effective probe volume length dimension (m)
micron	Micrometer or 10^{-6} meter
N_p	Total number of particles in the particle field (-)
$\bar{N}_{ph}$	Average or mean photon arrival rate (Hz)
N_λ, $N_\lambda(T)$	Spectral radiant intensity in the normal direction ($W \cdot m^{-3} \cdot sr^{-1}$)
$\bar{N}_\lambda(T)$	Value of $N_\lambda(T)$ averaged over the wavelength interval $\Delta\lambda = \lambda_2 - \lambda_1$ ($W \cdot m^{-3} \cdot sr$)

N'_λ	Spectral radiant intensity at an angle β relative to the surface normal ($W \cdot m^{-3} \cdot sr^{-1}$)
n	Number of photons received over some time interval; number of (photocathode electron) events detected as one thermal particle passes through one probe volume (-)
$\bar{n}$	Average or mean value of n (-)
n_p	Number of particles per unit volume (m^{-3})
PMT	Photomultiplier tube
$P_{(n,\tau)}$	Probability of n events over a time period τ with a Poisson distribution (-)
p	Total cone beam power (W)
p_b	Power radiated by the backdrop (background surface) in-line with both the virtual aperture and the aperture of the collecting lens system (so as to be collected and detected) (W)
p_p	Power radiated by the particle that is incident onto the detector (W)
RM	Rate monitor
SNR	Inherent signal-to-noise ratio of the photoelectron signal burst generated by a single particle (-)
SNR_{ph}	Inherent signal-to-noise ratio of the collected photon signal burst from a single particle (-)
s_f	Distance of object (fiber optic) from imaging lens system (m)
s_v	Distance of probe volume from imaging lens system (m)
T	Absolute temperature (^oK)
TEM_{mn}	Propagating electromagnetic wave with transverse electric and magnetic (TEM) fields and Gaussian intensity distribution
TEV	Thermal emission velocimeter
V1, V_1	Upstream probe volume region
V2, V_2	Downstream probe volume region
V_v	Volume of the principal or high collection efficiency region of the probe volume assuming $s_v >> D_\ell >> D_v$; detection volume or volume within which a particle must be to be detected (m^3)
v_p	Velocity of particle ($m \cdot s^{-1}$)
x_{pf}	x-axis or depth dimension of particle field (m)
x_{vb}	Distance between the probe volume and the backdrop surface (m)
x^{**}	Normalized x-axis coordinate of a single probe-volume-region coordinate system (-)
ZCD	Zero-crossing detector
Δz, Δz_v	Particle displacement distance corresponding to duration of TEV signal for one probe volume (m); z-axis probe-volume dimension (m)

z''	Normalized z-axis coordinate of a single probe-volume-region coordinate system (-)
z_{12}	z-axis distance between the upstream and the downstream probe volume (m)
α_b	Emissivity of backdrop surface (-)
$(1 - \alpha_b)$	Diffuse reflection coefficient of backdrop surface (-)
α_p	Emissivity of particle (-)
$\overline{\alpha}_p$	Detection-interval ($\Delta\lambda$)-averaged α_p (-)
β	PMT cathode photoelectron yield per joule of incident energy (j^{-1})
γ	Relative value of the beam power trigger level setting (of maximum value 1) (-)
η	Quantum efficiency (photocathode electrons per photon) (-)
θ	Divergence angle of radiation cone of Fig. 13 (r)
$\theta_{1,2}$	Angle between the probe volume axes (r)
θ_c	Angle of radiation collection; same as θ_v (r)
θ_v	Angle of a probe volume high-detectivity region; same as θ_c (r)
λ	Wavelength of thermal emission (m)
$\Delta\lambda = \lambda_2 - \lambda_1$	Wavelength band for which detection efficiency is 50 percent or greater (m)
λ_1	Lower wavelength limit for which detection efficiency is 50 percent or greater (m)
λ_2	Upper wavelength limit for which detection efficiency is 50 percent or greater (m)
$\lambda_{T\text{-}MAX}$	Wavelength corresponding to the peak (maximum) value of $N_\lambda(T)$ (m)
σ_{ph}^2	Variance in n (-)
τ	Signal period; time period (s)
Ω_c	Solid angle of radiation collection; $\pi\theta_c^2/4$ (sr)
Ω_c'	Relative radiation collection efficiency (of maximum value 1) (-)

THERMAL EMISSION VELOCIMETER

As previously mentioned, the HEAT facilities produce both an ablative and an erosive testing environment. Gas temperature and velocity are nominally 2000 to 5000°K and 1000 to 2000 $msec^{-1}$, respectively, and the small injected particles (of nominally 100 to 200-μm-diameter carbon material) are heated, ablated, and accelerated in the nozzle to temperatures, sizes, and velocities that are generally unknown until measured.

Streak photography using a high-speed camera, laser velocimetry, pulsed laser holography[1] and thermal emission velocimetry[2] have all been applied to measure the dust cloud parameters. Photographing the hot particles with a high-speed camera produced streak image recordings from which particle

velocity could be measured with ±15 to ±20 percent accuracy; such a technique has been used over the entire range of the fa lity operating conditions. A laser velocimeter (LV) that utilized four interference fringes, a 30-deg forward scattering angle, a high-power argon-ion laser, and a narrow bandwidth [1.0 nanometer (nm)] spectral filter (to reject the thermally emitted signal), produced good signals at low working gas temperatures (up to 2700°K). However, very little particle velocity data could be recorded as signal processing/recording instrumentation applicable to low-cycle-count LV signals was not then available. However, such an LV potentially can provide ±10 percent accuracy velocity data over all HEAT facility operating conditions if proper signal processing and narrower bandwidth spectral filtering are employed. The pulsed laser holographic recording technique,[1] using the HEAT arc jet as an optical diffuser and recording holograms on the jet far side, produced reconstructed particle images of marginal quality. More recently, the thermal emission velocimeter (TEV) technique[2] was employed to measure particle velocity through essentially the entire operating range of the HEAT facilities and with ±5 percent accuracy. The TEV was much simpler to build, operate, and maintain in comparison to the proposed LV system and produced similar results. It is now thought that the TEV technique can be expanded or a multiple-laser-beam technique (similar in principle to that of the particle rate monitor discussed herein) can be developed to permit total particle field parameter measurements to be made in the HEAT facility in the near future; such an effort is currently underway at AEDC.

TEV OPERATING PRINCIPLES

The thermal emissive velocimeter measures the velocity of hot particles by detecting the thermal radiation emitted by a particle when its trajectory carries it through each of two spatially separated probe volumes.

The TEV detection system shown in Figure 1 defines two regions or volumes in space, V1 and V2, that (1) are regions of maximum light collection (and detection) efficiency (Appendix A discusses light collection efficiency) and (2) are spatially separated by a known distance. That is, the electro-optical detection systems to the left in Figure 1 will detect a point source of light with high relative collection efficiency only when it lies within one of the two detection regions V1 and V2. Thus a hot particle moving along the z axis of Figure 1 through these regions while emitting thermal radiation will generate photodetected signal amplitudes versus particle spatial position as indicated in Figure 2. Knowledge of the spatial distance between the two detection volumes and the transit time between the two signal maxima permits a calculation of particle velocity.

Throughout the remainder of this article it will be assumed, unless otherwise stated, that the probe volumes and/or the particle number density are sufficiently small such that only one particle at a time is detected.

TEV OPTICAL DESIGN

The most common TEV optical design employed at the AEDC is illustrated in Figure 1, with an exception that many times only one photomultiplier tube (PMT) detector was employed to detect both optical signals (with both fiber-optic components directed to the common PMT). Two achromatic collimating lenses were employed back-to-back to first collect and collimate the radiated

signals, and then to focus the collimated signals onto the ends of two optical fibers. The fiber ends served as limiting apertures. The fiber optics collected the signals and transmitted them to the control room, at which point they were photodetected. Plastic fibers were used in the detector head where short radius bends were required, and glass fibers of high transmission efficiency were employed to transmit the signals to the detector(s). All of the fiber-optic components were single, continuous elements of 250-μm diameter. The high noise level of arc-current-induced electromagnetic radiation emitted by the HEAT facilities suggested that the photodetectors and other electronic instrumentation be located in the shielded environment of the control room, located 30 m from the arc heater.

The wavelength selectivity of the optical system components caused the overall system radiation detection efficiency to be very low, but, nevertheless, adequate for detection purposes. Even though the transmission bandwidth of the lenses and optical fibers (of nominally 400 to 1100 nm) approximately coincided with the peak of the spectral emission band of the thermal radiation (from the nominally 2000 to 4000°K particles, see Appendix A), the thermal emission bandwidth was approximately a factor of 4 larger than the transmission bandwidth of the optics. Furthermore, the bandwidth of the PMT detectors employed (which were existing detectors and not specially selected for the application) was very narrow (320 to 530 nm) and further reduced the optical system effective bandwidth by an additional factor of 8. Wide bandwidth PMT detectors are generally available with gallium arsenide photocathode material that has high responsivity over a 240- to 880-nm bandwidth.

TEV PROBE VOLUME GEOMETRY

The three-dimensional geometry of the probe volume can be scaled up or down by changing the diameter of the virtual aperture, D_v, through the equation $D_v = s_v s_f^{-1} D_f$, where the quantities in this equation are defined in Figures 1 and 11. If conventional spherical surface lenses are used with a circular aperture in axial symmetry, for $s_v \gg D_f \gg D_v$ (Figure 1) the volume of the optimal or high-collection efficiency region of the probe volume (the shaded region of Figure 1) is

$$V_v \cong \frac{\pi D_v^3}{6 \theta_c} \tag{1}$$

A TEV optical design that provides both the smallest probe region maximum (or length) dimension and minimal systematic measurement error is shown in Figure 3. Note that the probe volumes are not totally in line along the flow direction. Time periods would be measured as particles traversed between the two probe volumes as with the normal TEV. However, at the signal period $\tau = D_v v_p^{-1}$ there would occur an accumulation of signal data above the baseline data because of particles intercepting both probe volumes, thereby generating effective probe volumes of much smaller maximum dimension. The maximum length of the effective probe volumes is given by (see Figure 3)

$$L_v \cong \frac{n_v}{\sin\left[(\theta_{1,2} + \theta_v)/2\right]} \tag{2}$$

Note also that the probe volume centerlines are both parallel to the x' - y plane and therefore the normal (though usually small) systematic error associated with a nonuniform distance between the probe volumes is eliminated.

The concept that a relatively simple optical system (consisting of an imaging lens system and the single opening of an aperture) will collect point source radiation with high efficiency from only a small, definable region in space is fundamental to the design of a TEV and is outlined in Appendix B. Statement (2) of Appendix B, which identifies which rays will be collected, can be used to determine the probe volume geometry by way of collection efficiency contours. For the case of a circular aperture stop at the fiber optic and a circular lens system aperture stop, the single-probe-volume collection efficiency contours are x-axis symmetric as indicated in Figure 4a, which is a two-dimensional plot of contours of constant radiation-collection efficiency.

Two important probe volume geometries result when either one of the single-probe-volume aperture stops is changed from a circle to a narrow slit as illustrated in Figures 4b and c. Both are important to TEV design since they can be advantageously utilized as follows: (1) a reduction in the z-axis width of the aperture of the imaging lens system reduces the single-probe-volume signal duration for remote (or non-central) particle trajectories to correspond to $\Delta z \cong D_p + D_v$ particle displacement;* (see Figure 4b with particle trajectory parallel to the z-axis); (2) a reduction in the z-axis width of the aperture of the fiber optic reduces the single-probe-volume signal duration for central particle trajectories to correspond to $\Delta z \cong D_p$ particle displacement, assuming $\Delta z_v << D_p$.

Case (1) above, which can be used to reduce the z-axis widths of the remote regions of the two TEV probe volumes, represents the TEV geometry that is most often employed at AEDC. However, in one employment where much lower than usual accelerating gas temperature (and particle temperature) was expected, this slit aperture was not used, allowing the full circular collecting lens aperture to gather light and produce maximum signal amplitude. Signal broadened data, from the remote probe volume regions, were minimized by choosing only the particular data samples that resulted from the employment of relatively large trigger level settings on the electronic signal processor; (see the subsection "Computer Controlled Counter Method" of the section "TEV SIGNAL CONDITIONING AND DATA ACQUISITION" in this paper).

Case (2) above, which reduces the z-axis width of the central region of the probe volume, has not been utilized to date. However, such an employment can potentially be used in conjunction with a TEV to measure the z-axis dimension of a translating particle and may be used for this purpose some time in the future at AEDC. It is not difficult to envision a TEV-based system that simultaneously measures the velocity and two orthogonal dimensions of a translating particle.

---

*For very remote particle trajectories with finite (nonzero) lens aperture slit width, the signal duration slowly increases so that $\Delta z \cong D_p + D_v$ is not satisfied; in fact, $\Delta z >> D_p + D_v$ is satisfied. However, signals from such very remote probe volume positions are relatively very weak and therefore are usually ignored by an electronic signal processor.

C-5

Cases (1) and (2) above can be effectively used in conjunction, i.e., deployed in the same single-probe-volume optical system, to simultaneously achieve the benefits of both. However, it must be remembered that both cases contribute to a reduction of the total number of signal photons detected from a translating particle.

TEV EXTRANEOUS RADIATION SOURCES

Extraneous, noise-contributing radiations not received from the hot signal particles in the TEV probe volumes can be categorized as either (1) direct, line-of-sight radiation components from remote particles, from a radiating accelerating gas, and from a hot radiating backdrop surface (via rays through the detection volume virtual aperture in line with the collection aperture, see Appendix B), or (2) indirect radiation components (from particle field, accelerating gas, cell lights, or whatever) scattered off the backdrop and then through the same high-detectivity region of the probe volume in line with the detector optics aperture. The direct component that results from particles located in the remote, low-detectivity regions of the probe volume can be substantial to the point of obscuring the signal. Substantial obscuration would result, for example, if the particle field were dense enough such that because of particle blockage the detector could not see through to the relatively low-emittance backdrop. This condition would frequently occur without a particle being located in the high-detectivity region of the probe volume if $n_p \pi D_v^3 (6\theta_c)^{-1} < 1$ and $\exp(-x_{pf} n_p A_p) \ll 1$ where $\pi D_v^3 (6\theta_c)^{-1}$ is the assumed approximate volume of the high-detectivity region of the probe volume and $(n_p A_p)^{-1}$ is the mean free path of a light ray propagating through the particle field.

The indirect components of detected radiation result from radiation being scattered off the (assumed) diffusely reflecting backdrop. These components cannot usually be eliminated by reducing the diffuse scattering coefficient of the backdrop to a negligible value as (1) most low-scatter, high-absorbing optical surfaces, such as flat black paint or black optical felt, will diffusely scatter at least a few percent of the incident radiation and (2) a high spectral reflectivity or mirror surface, which will scatter typically a few tenths of one percent, only reflects or deviates the line of sight of the detector package to another backdrop surface, and does not by itself provide a solution.

The relative detection of a particular extraneous radiation component is governed, in part, by the position in space from which it originated; the collection efficiency analysis of Appendix B can be used to determine the relative contribution versus spatial position of any component. For example, it can be shown that if the number of particles that illuminate the backdrop originate from a relatively small (in comparison to x_{vb}) bounded region, then the radiated particle field component that is diffusely reflected off the backdrop is negligible (relative to signal) if[2]

$$x_{vb}^2 \gg A_v (1 - \alpha_b) N_p/\pi \tag{3}$$

In this equation, x_{vb} is the distance between the probe volume and the backdrop surface, A_v is the probe-volume virtual-aperture area, $(1 - \alpha_b)$ is the

(assumed) diffuse reflection coefficient at the backdrop, and N_p is the total number of particles in the particle field (radiating at the backdrop).

Detection Conditions

For a TEV system employing a high-responsivity photomultiplier tube and a time-interval counter type of signal processor to effectively extract data, the following conditions must be met: (1) the detected thermal radiation quantum number (photons) resulting from a single particle traversing the high-detectivity region of a probe volume, assuming no background radiations are present, must be great enough to produce large inherent signal-to-noise ratio (or SNR, see Appendix C); (2) the mean detected level of background radiation (photons/second), assuming no principal particle is present, must be significantly less than the detection level when a principal particle is present, and (3) the particle number density, n_p (assumed uniform over a depth x_{pf}), must be low enough such that $n_p << V_v^{-1} + (\bar{A}_p\ x_{pf})^{-1}$, where V_v is the volume of detection** of a single TEV-probed region, $\bar{A}_p$ is the mean particle cross-sectional area, and x_{pf} is the x-dimension or depth of the particle field.

If the above detection conditions are not met, it is doubtful that a time-interval counter (signal processor) can be effectively employed; however, in some cases, other signal-processing means, more capable of extracting periodic data from noisy environments, may possibly be used. For example, if condition 1 is not met but the inherent single particle SNR is low and of approximate value SNR $\cong$ 1, then a correlation type of signal processor would provide a good opportunity to extract data from the near side of a particle field, regardless of conditions 2 and 3. For condition 1 with SNR << 1, conditions 2 and 3 must be approximately met for even a correlator type to extract data in a reasonable time.

TEV SIGNAL CONDITIONING AND DATA ACQUISITION

Moving Pictures of Oscilloscope Method

The initial means of processing and acquiring TEV data was to take movie pictures of the signal displayed on an oscilloscope. The optical signals from the two probe volumes were detected on a common photomultiplier tube (PMT) detector. A very sensitive movie film (ASA 400 color film, push processed to ASA 800), a movie camera optimized for low light level, and an oscilloscope designed to record high-speed, single-swept events were used to record TEV data. The scope was operated in a single horizontal (time) sweep mode with the (normally manually controlled) horizontal sweep reset command signal being automatically delivered by, and synchronized to, the movie camera. To accomplish the latter, a circuit was developed that automatically rearmed the oscilloscope horizontal sweep immediately upon each opening of the movie camera shutter. After each rearming, the first signal (if any) meeting the qualifications of the oscilloscope trigger circuit would be displayed on the CRT and recorded on film. Utilizing this method, individual TEV signal events were recorded at the frame rate of the movie camera, nominally 15 to 75 frames per second.

**The detection volume or probe volume is the volume within which a particle must be to be detected.

Computer-Controlled Counter Method

The final choice of a TEV signal-processing and data-acquisition system consisted basically of a 20-picosecond resolution programmable electronic counter, a crystal-controlled general purpose lectronic timer, a flexible disk magnetic storage device, and a graphics display terminal, all interfaced to a microcomputer. The counter was operated in the time interval measurement mode to process TEV signals and its start-stop channel trigger levels were programmed by the microcomputer. The timer was started at the beginning of a data run to correlate acquired data with time.

Such a system provided the major benefits of (1) automatic progression during a run through a range of trigger levels sufficient to obtain TEV data under most tunnel conditions, (2) acquisition and storage of data at high rates, and (3) automatic reduction and plotting of data following the run. The computer was programmed to stop and acquire data at each trigger level for a time that was sufficient (e.g., 0.1 sec) to obtain a large data sample. The typical HEAT facility run time was only a few seconds. Without automatic, step-by-step ranging of the trigger levels during a run, a few (unnecessary) preliminary runs would be required to establish trigger levels for each new set of arc heater conditions.

A microcomputer with 28k 16-bit words of memory was used to control the counter trigger levels and to acquire, store, and display the counter and timer data (Figure 5). TEV time-interval-counter data and timer data were stored on the magnetic flexible disk for permanent retention and were later reduced, displayed, and copied in a velocity histogram format.

Figure 6 is a flow chart of the computer program used to control trigger levels and acquire TEV data. A combination of Fortran and assembly language programming was used to implement this flow chart. Trigger levels are changed by factors of two (40 mV, 80 mV, 160 mV, etc.) every 100 msec during a run. Each time a new trigger level is selected, information on the memory location where data from the previous trigger level was stored is maintained so that data can later be analyzed by trigger level. After seven levels have been programmed (700 msec), the sequence of trigger levels repeats. This sequencing allows at least some data to be recorded throughout the run regardless of signal level variations. Following an initial data run to establish the range of pulse heights, the number and range of trigger levels programmed may be reduced.

Data from the TEV time-interval counter was rounded to the nearest nanosecond and stored in computer memory as a 16-bit unsigned integer in the range 0 to 65535 nsec. The value of run time from the general purpose timer was stored to a resolution of 10 msec as another 16-bit integer. However, to conserve memory, run time was only stored with every tenth TEV reading. The average time required to read and store a single TEV reading was 600 μsec, which permitted in excess of 100 readings to be obtained at each programmed trigger level provided the rate of TEV pulses was adequate. Data were stored in computer memory until either the maximum run time programmed had elapsed or until 15,000 TEV readings (memory capacity) had been acquired. The TEV data were then recorded onto flexible disk and, if desired, read back and processed for display by trigger level. A typical TEV velocity histogram is shown in Figure 7.

PARTICLE RATE MONITOR

The Dust Erosion Tunnel (DET) generates a high-velocity (1000 to 3000 $msec^{-1}$) dust cloud of large cross-section (0.1- to 0.4-m diameter) and low number density (resulting from 100 $gm \cdot sec^{-1}$ maximum, particle mass injection). The mean particle size ranges from a few tenths of a millimeter to one millimeter average dimension (the particle shape is irregular, nonspherical). Optical access to the test section is provided by pairs of opposing windows viewing transversely through the dust cloud jet with one window on each side of the test section.

Over the years, various optical instrumentation techniques have been used to calibrate the DET particle fields. A pulsed laser holographic technique[1,3] was employed to measure particle size, velocity, and number density; a laser velocimeter[4] measured particle velocity; and an optical fiber-optic technique[5] was used to measure particle size. Much of this data is summarized in a report describing the DET facility and its calibration.[6] More recently, an optical particle rate (number/time) monitor (or RM) was employed that measured the instantaneous local particle rate throughout a run by photodetecting and counting the number of beam power reductions as particles intercepted a small laser beam. This instrument provided data for a nominally 3:1 particle size range, and it is believed that two of these instruments would provide data over the full 10:1 range of mean particle size that is characteristic of the DET facility operation. Furthermore, recent results indicate that by separately photodetecting the interruptions of many closely spaced, small laser beams by individual particles, size and velocity as well as relative contribution to rate per unit area can be measured. The particle rate monitor instrumentation will now be described.

RATE MONITOR OPERATING PRINCIPLE

The particle rate monitor employs a laser beam of special geometry that is transmitted through the DET particle field. Individual particles of the low-number-density particle field intercept the beam and produce transient reductions of beam power. These are detected and counted using a photomultiplier tube (PMT), a special pulse-discriminator circuit, and an electronic counter operating in the event-counting mode. Individual particle interruptions are counted over fixed intervals of time, and accumulated count data and time data are periodically recorded on the magnetic tape of a microprocessor-based graphic display unit.

RATE MONITOR PERFORMANCE CHARACTERISTICS

The optical geometry of the particle rate monitor beam is shown in Figure 8. A truncated-cone-geometry laser beam (see Appendix D for particle rate monitor optics) converges to a minimum diameter disk slightly smaller than the smallest particle size to be detected. The beam then diverges symmetrically about the minimum diameter. The point of minimum cone diameter is positioned in front of a model being tested. The detection cross section, or the area through which a particle center must pass to be detected, is based on a particle blocking a specific minimum fraction (50 percent or more, for example) of the laser beam; the detection cross section of both a small and a large spherical particle is indicated in the figure. For a particle to be detected,

the center of the (assumed spherical) particle must intercept the detection cross section or detecting area.

It is advantageous that the detection cross section increases as particle size increases. This is because particles of larger (mass weighted) mean size can be injected only at lower (number per second) rates and therefore require a larger detection cross-section to accumulate a large data sample in a given time. Also, one beam geometry can be effectively employed for a range of particle sizes. To date for the DET application a 500-μm, or micron, cone minimum diameter has been used to detect chiefly in the 400- to 1000-micron range.

For design purposes it is necessary that the cone minimum diameter be an appreciable fraction of the (mass-weighted) mean particle size so that the many small particles usually present in a sample having a large mean particle size will be discriminated out and not detected. Otherwise the possibility would exist that the accumulated count data would not be representative of the large particles that dominate the model erosion process.

The convergence-divergence angle of the cone beam is also important. First it determines, in part, the detection cross section that must be large enough to obtain a large number of particle counts per sampling interval. It should be noted that the relative (reduction in beam power) trigger level also determines the detection cross section. Secondly, a significant cone angle limits the longitudinal dimension of the detection cross section, permitting monitoring of particle rate in an area of flow more representative of an immersed test model than the entire flow area.

Inherent Signal-to-Noise Ratio

Assuming that the detected level of background radiation is negligible relative to the RM beam power, then accurate RM count data are obtained if the RM beam power at detection, γp, produces a high inherent signal-to-noise ratio (SNR >> 1). The effective detection time interval is determined by the electronic bandwidth, Δf, of the threshold trigger circuit of the electronic counter. The intrinsic or inherent SNR is thus (see Appendix C)

$$SNR = (\gamma p \beta / \Delta f)^{\frac{1}{2}} \tag{4}$$

where γ is the beam power trigger level setting relative to the total cone beam power p, and β is the PMT cathode photoelectron yield (photoelectrons per joule). For example, an SNR of 20 is generated with a 50-percent trigger level ($\gamma = 0.5$) of a $P = 10^{-5}$ watt beam with $\Delta f = 10^{8}$ Hz and $\beta = 10^{16}$ per joule.

RATE MONITOR SIGNAL CONDITIONING AND DATA ACQUISITION

Initially, to acquire data with the particle rate monitor system, a zero-crossing detector (ZCD) was used to compare the instantaneous PMT signal voltage to a fixed-reference voltage; the ZCD outputted a level change when the two voltages became equal. ZCD output level changes were electronically counted over fixed time intervals to produce rate monitor data. A commercially available, IEEE-488 bus-compatible, electronic counter operating in an event-counting mode was employed. However this initial system was not satisfactory as it produced inconsistent data.

The cause of the data inconsistency was due to two undesirable characteristics in the PMT detector output signal. These were (1) included broadband electrical noise attributable in part to the moderate signal-to-noise ratio of the detected optical signal (quantum noise) and in part to the included electrical noise induced by the nearby 5-MW arc heater (generating the facility flow) and (2) the problem of window contamination buildup, which resulted in attenuation of the signal beam and a slow decrease of the mean signal level detected during a run. It was necessary that both problems be compensated for in order to extract optimum usable information.

The tunnel windows, which provided optical access to the test cell, slowly became contaminated during the run. The rate of this contamination was not necessarily constant, resulting in a detected beam power that continually decreased in an unpredictable manner, often to only 25 percent or so of the original pre-run values. Since the events to be detected were also characterized by a partial beam blockage and a corresponding detection level change, some means to discriminate between the two events had to be developed. A characteristic of the events that differed significantly between the two was the relative time duration of each, the drop in signal caused by a particle blockage occurring over a much shorter time than the gradual attenuation of the signal attributable to window contamination. A circuit was therefore developed to supply to the ZCD a varying threshold or reference voltage equal in amplitude to a percentage (corresponding to beam blockage by a spherical particle of a given size or larger) of the time-averaged, low-pass-filtered signal level. This effectively caused the attenuation of the beam caused by window contamination to be invisible to the ZCD's.

The other undesirable characteristic, that of a moderate level of broadband noise on the signal attributable chiefly to the low optical power of the signal beam in the early prototype RM system, was dealt with by employing lens L1 of Figure 13 and by adding variable hysteresis to the ZCD circuitry. The relative amount of hysteresis, again as a percentage of the variable low-pass-filtered PMT signal level, was selectable by setting two 10-turn potentiometers.

The data acquisition system for the particle rate monitor consisted of a graphic microcomputer system and two electronic counters operated in an event-counting mode, interconnected by an IEEE-488 bus. One counter was connected to the signal-conditioning electronics and maintained a running total of valid events (particles blocking a predetermined percentage of the beam). The second counter had as its input a 10-MHz clock and functioned as a time reference. The microcomputer read the contents of both counters approximately four times per second and stored the information on magnetic tape.

Typical rate monitor data is shown in Figure 9. Note that the dust was turned on and off periodically during a run as different models were injected into the test region. The RM data showing large fluctuations in dust rate from model to model have correlated well with net model erosion measurements taken after a run.

APPENDICES

A. Thermal Emission and TEV Signal

The characteristics of the thermal radiation emitted by a blackbody will be briefly outlined. The results will be applied in a subsequent section to define the thermal signal and thermal noise components.

Thermally emitted blackbody radiation is characterized by a Lambertian or cosine distribution of power versus angle between the radiation direction and the surface normal, i.e.,

$$N_\lambda' = N_\lambda \cos \beta \tag{5}$$

where β is the angle between the radiation N_λ' and the surface normal. N_λ (power $\cdot$ area^{-1} $\cdot$ wavelength^{-1} $\cdot$ solid angle^{-1}, or W $\cdot$ m^{-3} $\cdot$ sr^{-1}) is the monochromatic thermal radiation intensity in the normal direction, given by Planck's law

$$N_\lambda = C_1 \lambda^{-5} \left(\exp \frac{C_2}{\lambda T} - 1 \right)^{-1} \tag{6}$$

where T (^oK) is the absolute temperature, λ (cm) the monochromatic wavelength, $C_1 = 1.190 \times 10^{-12}$ watt $\cdot$ cm^2, and $C_2 = 1.439$ cm $\cdot$ ^oK. Equation (6) is plotted in Figure 10.

With the aid of Equation (5) it can be shown that a small radiating elemental area observed at an oblique angle β is equivalent to a reduced (by a factor cos β) projected area emitting along its surface normal. Therefore, for example, a small spherical blackbody (for example, a TEV thermal particle) will radiate as if it were a blackbody disk of the same diameter as the sphere and with the normal-to-the-disk surface parallel to the observation direction.

For a particle in the high radiation-collection-efficiency region of a probe volume (see Appendix B), the thermal signal power incident on the detector is given by, assuming $D_p \leq D_v$ (see Figure 11),

$$P_p = \Omega_c A_p \int_0^\infty \alpha_p N_\lambda(T_p)\, d\lambda \cong \Omega_c A_p \int_{\lambda_1}^{\lambda_2} \alpha_p N_\lambda(T_p)\, d\lambda \cong \Omega_c A_p \bar{\alpha}_p \bar{N}_\lambda(T_p) \Delta\lambda \tag{7}$$

where $\Omega_c \cong \pi\theta_c^2/4$ is the solid collection angle of the detector optics, A_p is the cross-section or projected area of radiation of the particle ($A_p = \pi D_p^2/4$ for a spherical particle), α_p is the particle emissivity, $N_\lambda(T_p)$ is the particle monochromatic thermal radiation intensity in the normal direction, λ_1 and λ_2 ($\lambda_2 > \lambda_1$) are the wavelengths at which the overall detection efficiency (or product of detector quantum efficiency and optical system transmission coefficient) of the TEV drops below 50 percent, $\Delta\lambda = \lambda_2 - \lambda_1$, and the raised bar notation denotes average value over the wavelength interval $\Delta\lambda = \lambda_2 - \lambda_1$.

B. Radiation Collection Efficiency

The purpose of this appendix is to review, very briefly, the radiation-collection efficiency of an imaging lens pair followed by a circular transmission aperture such as a fiber-optic component. More thorough reviews can be found elsewhere.

The optical system to be discussed is shown in Figure 11. A pair of positive lenses, of the achromatic point source collimating type, will be used to represent a simple form of a general type of high spatial resolution, achromatic, imaging system. Assume that points 1, 2, 3, and 4 to the right of the imaging lenses are point sources of light; these will image then to points 1′, 2′, 3′, and 4′ to the left of the lenses such that all (of the infinity of) rays from point 2, for example, that intercept the aperture of lens L1 will be directed by the lenses to pass through point 2′. Ray traces such as these can be employed to show the following: (1) that points within the shaded region 1, 2, 3, 4 image to points within the shaded region 1′, 2′, 3′, 4′ such that the former region is a region of high (point source) radiation-collection efficiency, so high in fact that all rays from a point within this region that also intercept the aperture of lens L1, will pass through aperture A′ and be collected; (2) any ray, directed from right to left, that is in-line with the (virtual hole in the) virtual aperture A and the aperture of lens L1, will be redirected by the lenses to pass through the real aperture A′ and be collected; any right-to-left ray that does not meet these criterion will intercept the opaque (non-hole) portion of aperture A′ and therefore will not be collected.

A thorough comprehension of these statements, in conjunction with elementary ray-tracing techniques, will permit one to compute surfaces of constant radiation-collection efficiency for the region to the right of the lenses. A quadrant of such a contour diagram is illustrated in Figure 12 for the case of circular (x-axis symmetric) optical components and assuming $s_v >> D_\ell >> D_v$, which is typical of many geometries. For $s_v >> D_\ell >> D_v$ the contour plot is symmetric also about the z-axis, and therefore all four quadrants would plot identically. The coordinates of Figure 12 are normalized such that

$$x'' = \frac{D_\ell}{D_v s_v} x \text{ and } z'' = \frac{2}{D_v} z \tag{8}$$

The relative radiation collection efficiency, Ω_c', plotted in Figure 12 is related to the actual effective radiation-collection solid angle, Ω_c, by

$$\Omega_c' = \frac{4 s_v^2}{\pi D_\ell^2} \Omega_c \tag{9}$$

again assuming $s_v >> D_\ell >> D_v$.

C. Inherent Signal-to-Noise Ratio (SNR)

Because of the statistical nature of the number of photons detected during the passage of a thermal particle through a TEV probe volume, for example, the TEV signal amplitude is inherently uncertain and noisy. The relative magnitude of such inherent noise will now be discussed.

For the TEV, the photon flux impinging on the PMT photocathode originates from a thermal broadband source and the photons can be assumed to be emitted at random time intervals. Under such conditions the probability that n photons will strike the photocathode in a time interval τ is given by a Poisson distribution as follows:[7]

$$P_{(n,\tau)} = \frac{(\overset{\circ}{N}_{ph}\,\tau)^n}{n!} \exp\,(-\overset{\circ}{N}_{ph}\,\tau) \tag{10}$$

where $\overset{\circ}{N}_{ph}$ is the average photon-arrival rate. The average value for n and the variance in n, σ^2_{ph}, can be obtained directly from $P(n,\tau)$ as:[7]

$$\bar{n} = \overset{\circ}{N}_{ph}\,\tau \tag{11}$$

$$\sigma^2_{ph} = \overset{\circ}{N}_{ph}\,\tau = \bar{n} \tag{12}$$

The inherent photon flux signal-to-noise ratio, $\bar{n}/\sigma_{ph}$, is given by

$$SNR_{ph} = (\overset{\circ}{N}_{ph}\,\tau)^{1/2} \tag{13}$$

and the inherent cathode photoelectron SNR for a single TEV particle pulse is given by

$$SNR = (\eta\,\overset{\circ}{N}_{ph}\,\tau)^{1/2} = \left[\beta\,N_\lambda(T_p)\,\alpha_p\,A_p\,\Omega_c\,\Delta\lambda\,(D_p + D_v)\,v_p^{-1}\right]^{1/2} \tag{14}$$

where η (dimensionless) is the photocathode quantum efficiency, $N_\lambda(T_p)$ ($W \cdot m^{-3} \cdot sr^{-1}$) is the monochromatic blackbody radiation intensity discussed in Appendix A, A_p (m^{-2}) is the particle cross-section or projected area of radiation ($A_p = \pi D_p^2/4$ for a spherical particle), Ω_c (sr) is the solid collection angle, $\Delta\lambda$(m) is the spectral detection bandwidth of the optics and detector, and $\tau = (D_p + D_v)\,v_p^{-1}$ is the time duration of the TEV signal pulse for a particle of diameter D_p and velocity v_p passing through a high detectivity probe volume region of diameter D_v.

The amplification or multiplication of the cathode photoelectron current in the PMT dynode chain is essentially noise-free. The use of high-gain PMT in conjunction with a low-pass filter of bandwidth $\tau^{-1} = (D_p + D_v)^{-1}\,v_p$ and a low-noise amplifier (if necessary)† ensures that the cathode photoelectron SNR is preserved to within a factor of two at the filter (or amplifier) output.[7] During the occurrence of the signal pulse (with the particle approximately centered in the probe volume for SNR >> 1) the filter (or amplifier) output voltage level will achieve a mean peak value and an average variance of the peak that provide a voltage ratio SNR that is within a factor of two of the

†A signal amplifier is usually necessary with low photoelectron SNR (SNR < 10) depending on the input voltage level requirements of the signal processor.

charge ratio SNR that appeared in the PMT cathode and plate electron currents. Thus, the quantum nature of the photon flux from a detected TEV particle causes an inherent photon flux SNR; this SNR is then reduced by a factor η upon photodetection and then approximately preserved through the electron multiplication, electronic amplification, and low-pass-filtering processes.

D. Particle Rate Monitor Optics

The particle rate monitor optical system that generated and detected the cone beam is shown in Figure 13. A 0.005-w helium-neon laser source (S) of 0.6328-μm wavelength, emitted a TEM_{00}, approximately collimated, continuous-wave laser beam of nominally 0.6-mm diameter. The laser illuminated, by way of lens L1, a piece of light-diffusing tape, D. The diffusing tape was Scotch® † tape No. 810, the commonly used office type that could be written upon. The tape scattered and absorbed all of the incident light with approximately 0.4 percent (20 μw) scattered into a principal low-divergence, forward-scatter cone of approximately θ = 0.2-radian divergence angle. This then intercepted a 100-μm diameter, centered circular aperture A1. It should be noted that the lens L1 focused the gaussian laser beam to a spot diameter that was smaller than the aperture A1 (to the focus point 2 of Figure 13), and that the distance between L1 and the diffuser-aperture (D-A1) combination was varied so that the aperture diameter was fully illuminated with approximately 40 percent of the power scattered forward in the principal lobe intercepting the aperture A1. The aperture A1, in conjunction with the very closely located diffuser tape D, effectively created a disk of point sources that was imaged by way of lens L2 and aperture A2 (which controlled the cone convergence-divergence angle), out into the test section to a 500-micron disk (of focused or imaged point sources). Lens L3 reimaged the cone beam onto a photomultiplier tube. Aperture A3 and the laser line (spectral) filter LLF were employed to reject radiation from test cell camera lights.

REFERENCES

1. Belz, R. A. and Menzel, R. W. "Particle Field Holography at Arnold Engineering Development Center," Optical Engineering, Vol. 18, No. 3, May-June 1979.

2. Brayton, D. B. "Velocimetry of Hot Particles by Detection of Thermal Emission," presented at the 25th International Instrumentation Symposium on Aerospace Test Measurements, sponsored by the Instrument Society of America, May 7-10, 1979. (Paper did not appear in the published proceedings; however, copies were made available to conference attendees).

3. Trolinger, J. D. and Belz, R. A. "Holography in Dust Erosion Facilities," AEDC-TR-73-160 (AD766420), September 1973.

4. Cline, V. A., Jr. "Dust Particle Velocity Measurements Using a Laser Velocimeter," AEDC-TR-72-159 (AD752225), December 1972.

5. Bentley, H. T., III "Fiber Optics Particle Sizing System," AEDC-TR-73-111 (AD766647), September 1973.

---

†Registered trade mark of the Minnesota Mining and Manufacturing Co.

6. Lewis, H. F., et al., "Description and Calibration Results of the AEDC Dust Erosion Tunnel," AEDC-TR-73-74 (AD910291L), May 1973.

7. Photomultiplier Manual, Theory, Design, Application, Technical Series PT-61, RCA Corporation, Harrison, N. J. 07029, September 1970, p. 56-76.

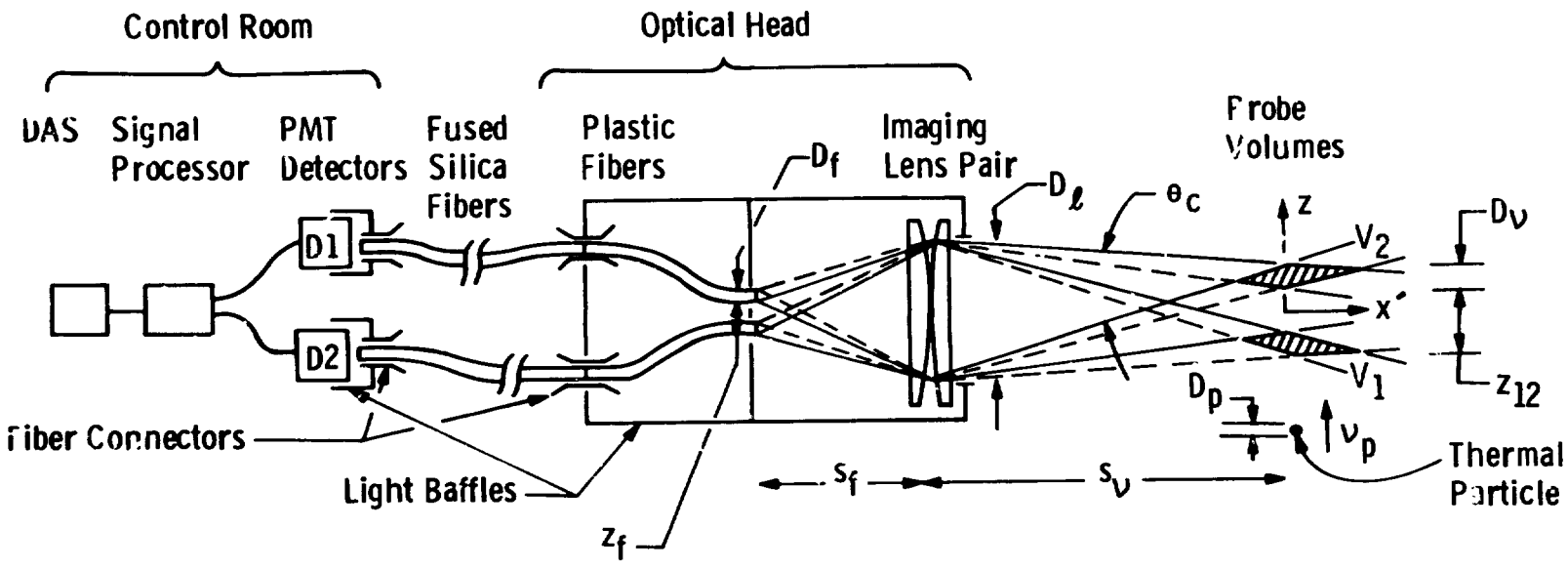

Figure 1. Thermal Emission Velocimeter

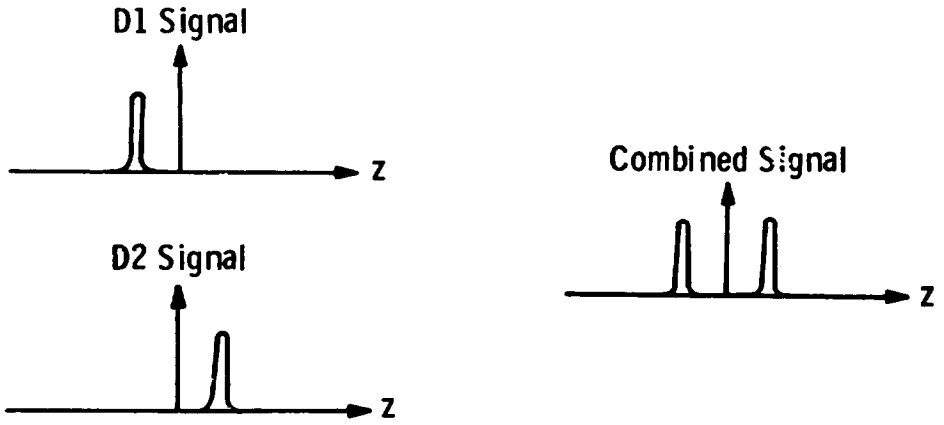

Figure 2. Detected Signal Amplitudes versus Particle Position

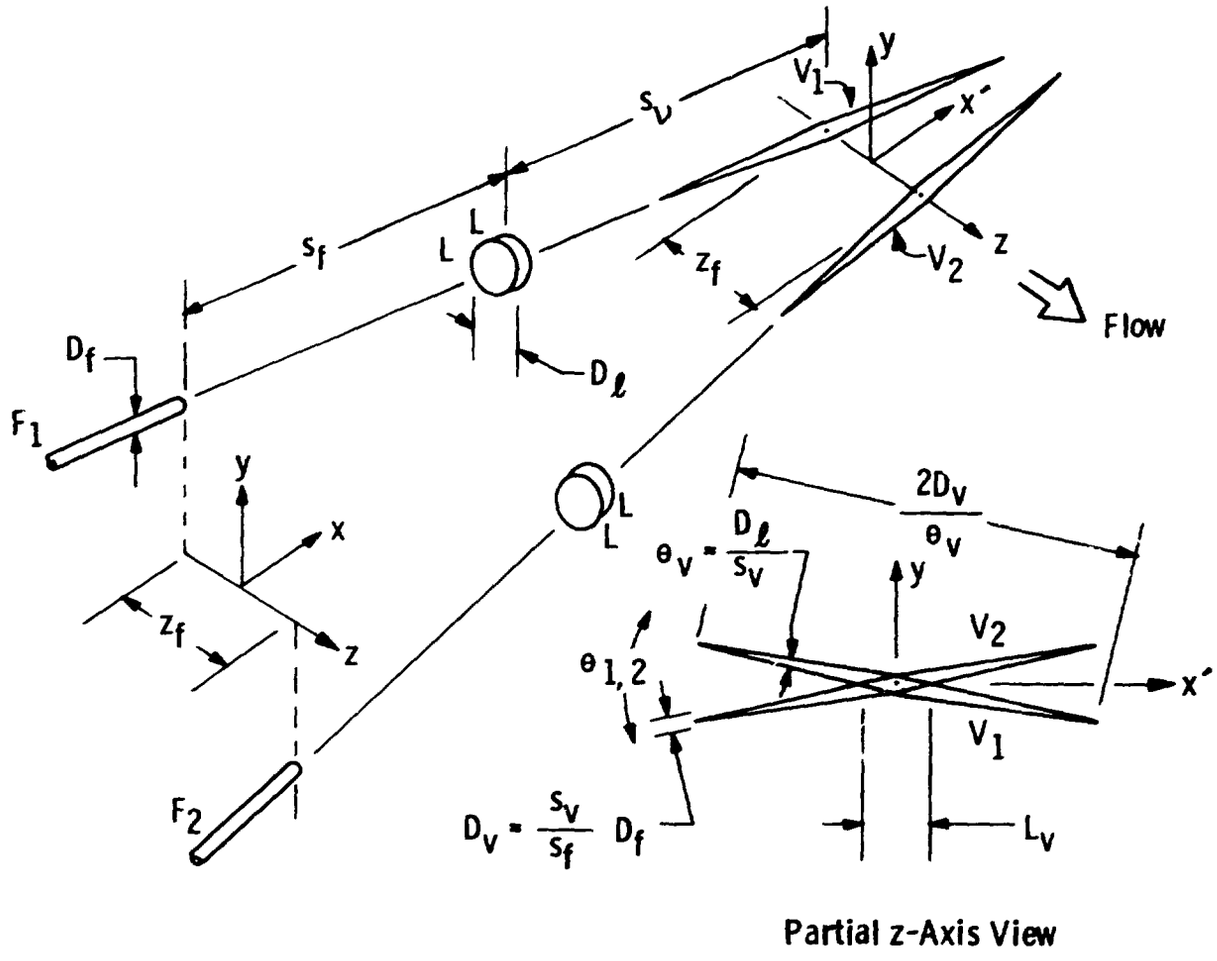

Figure 3. TEV Geometry Configured for Small Probe Volume Length and Minimal Systematic Measurement Error

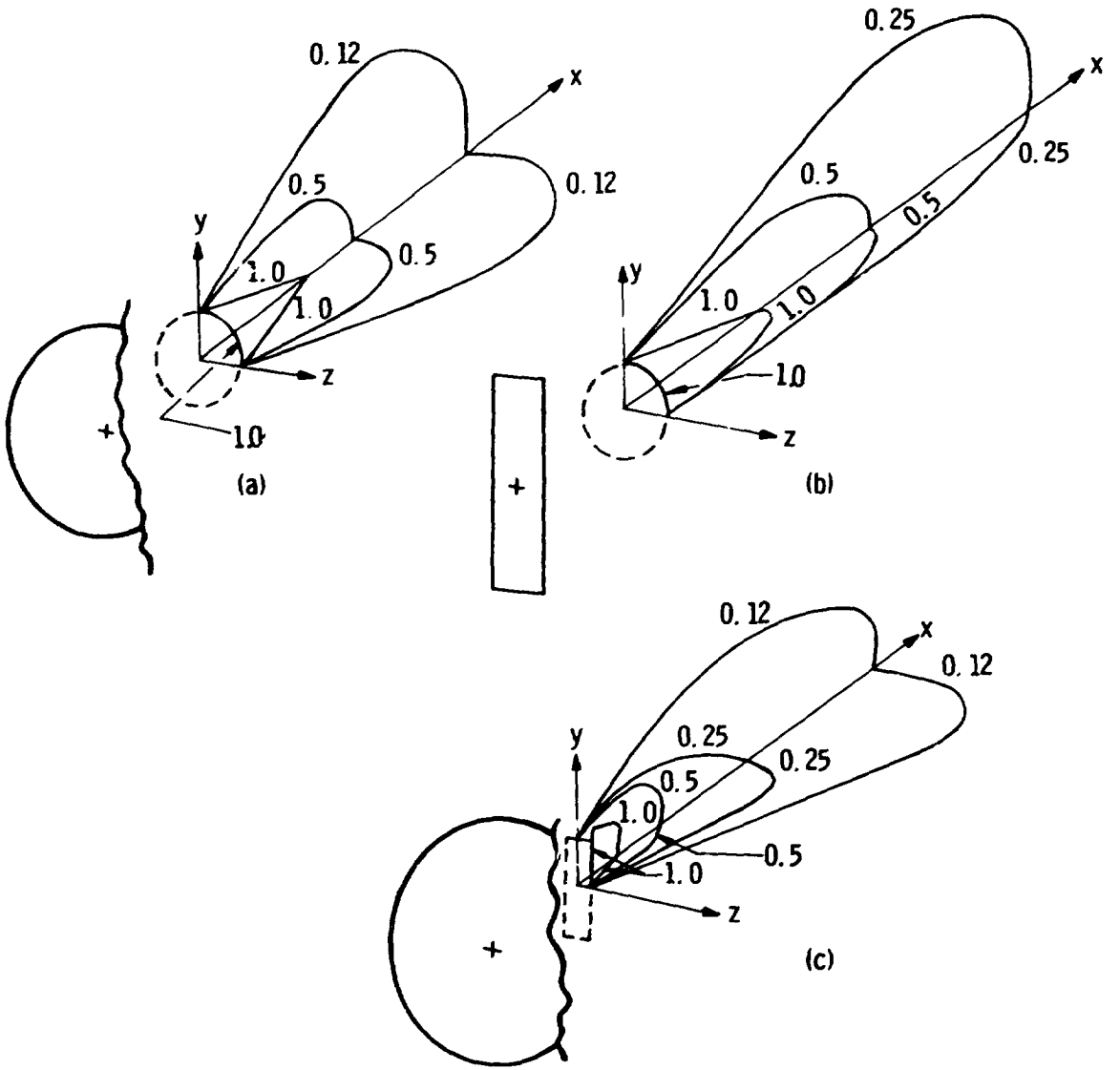

Figure 4. Approximate Radiation Collection Efficiency Contour Plots for Three Different Geometries of Collecting Lens Aperture and Virtual Aperture

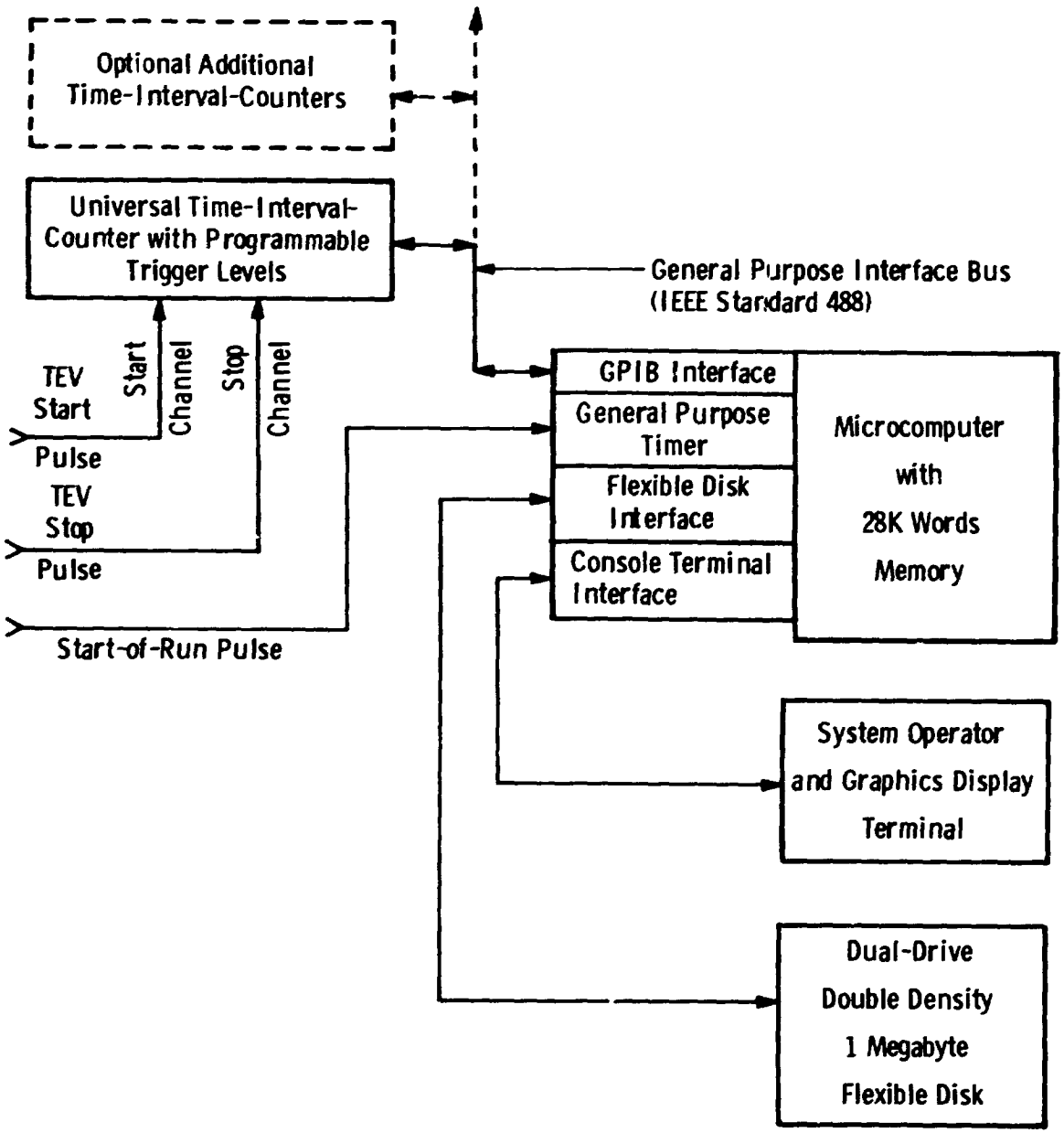

Figure 5. Data Acquisition System

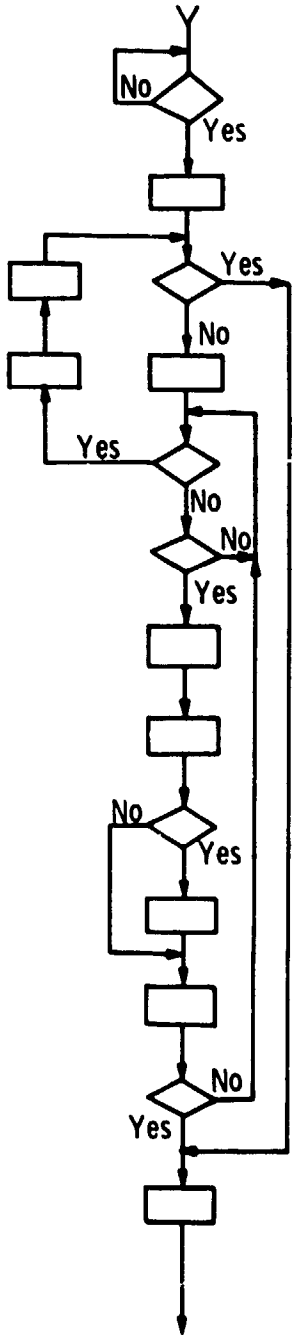

*Trigger Levels Repeat in Cycles of 7.

Figure 6. TEV Data Acquisition Program Flow Chart

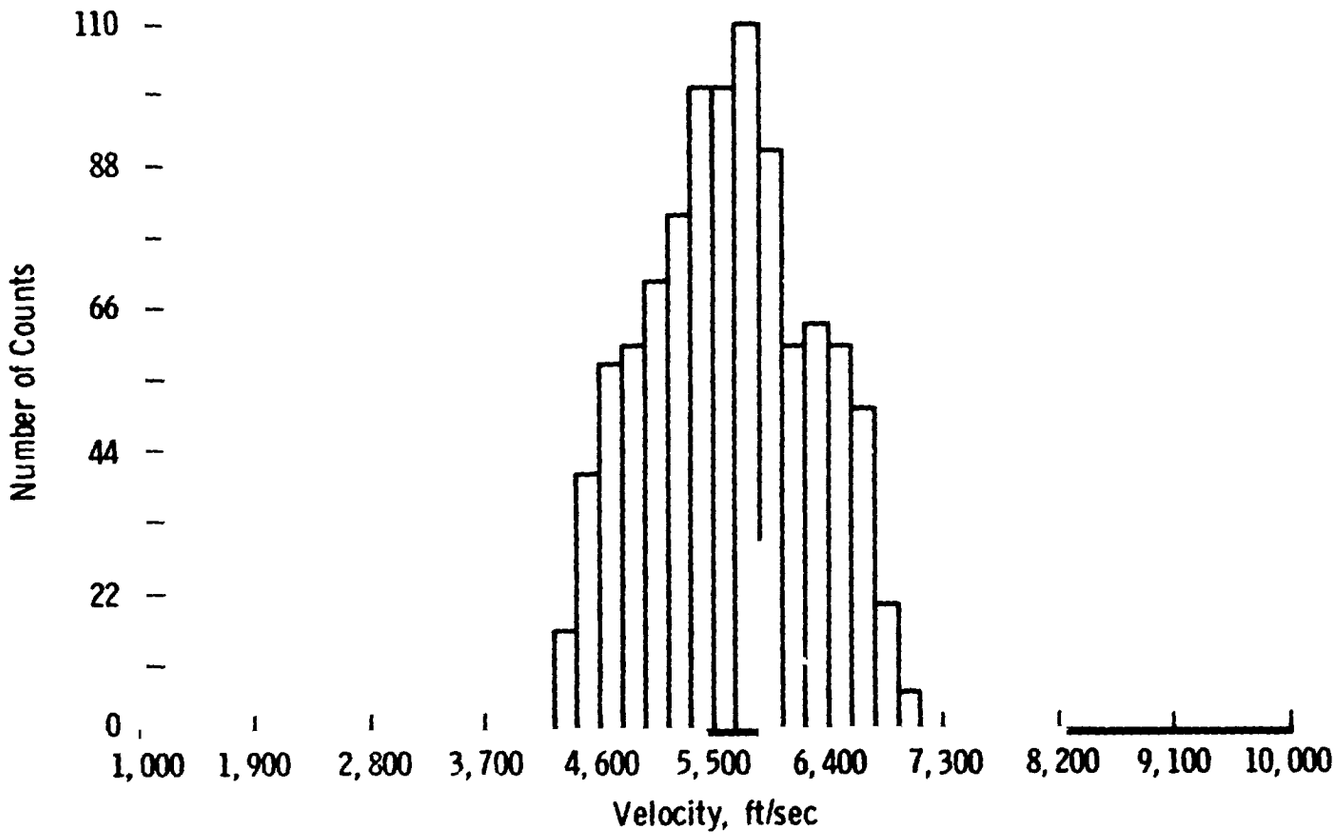

Figure 7. Typical TEV Data

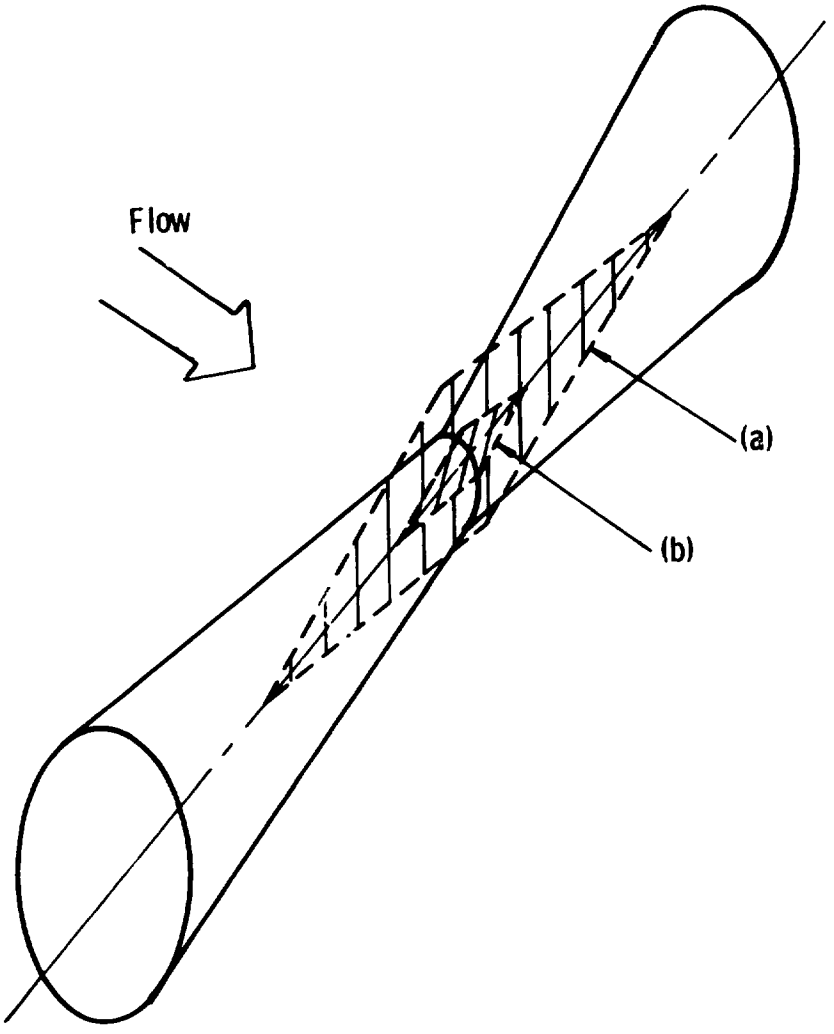

Detection Cross-Section
(a) for large particle
(b) for small particle

Figure 8. Particle Rate Monitor Beam

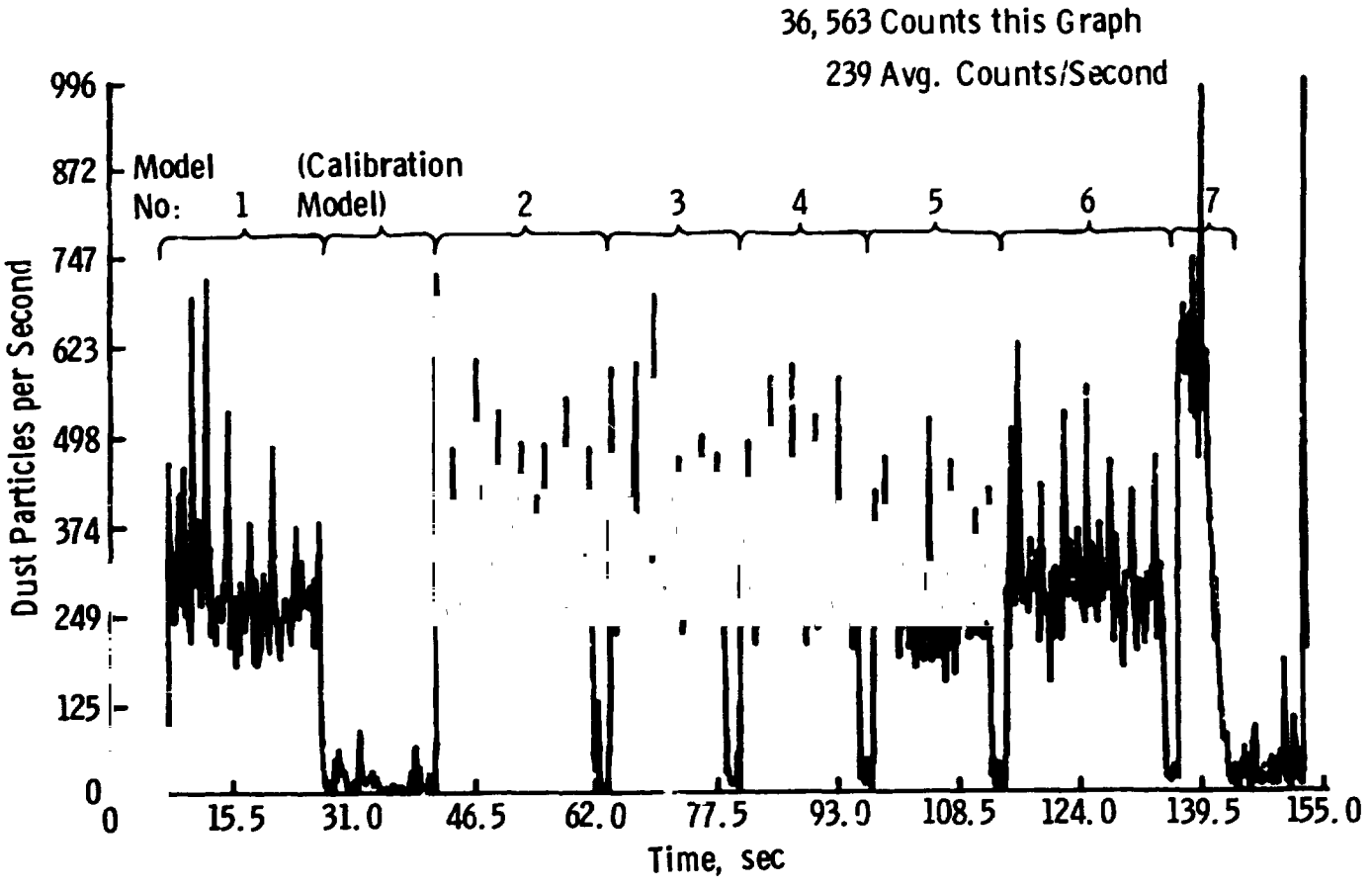

Figure 9. Typical Rate Monitor Data

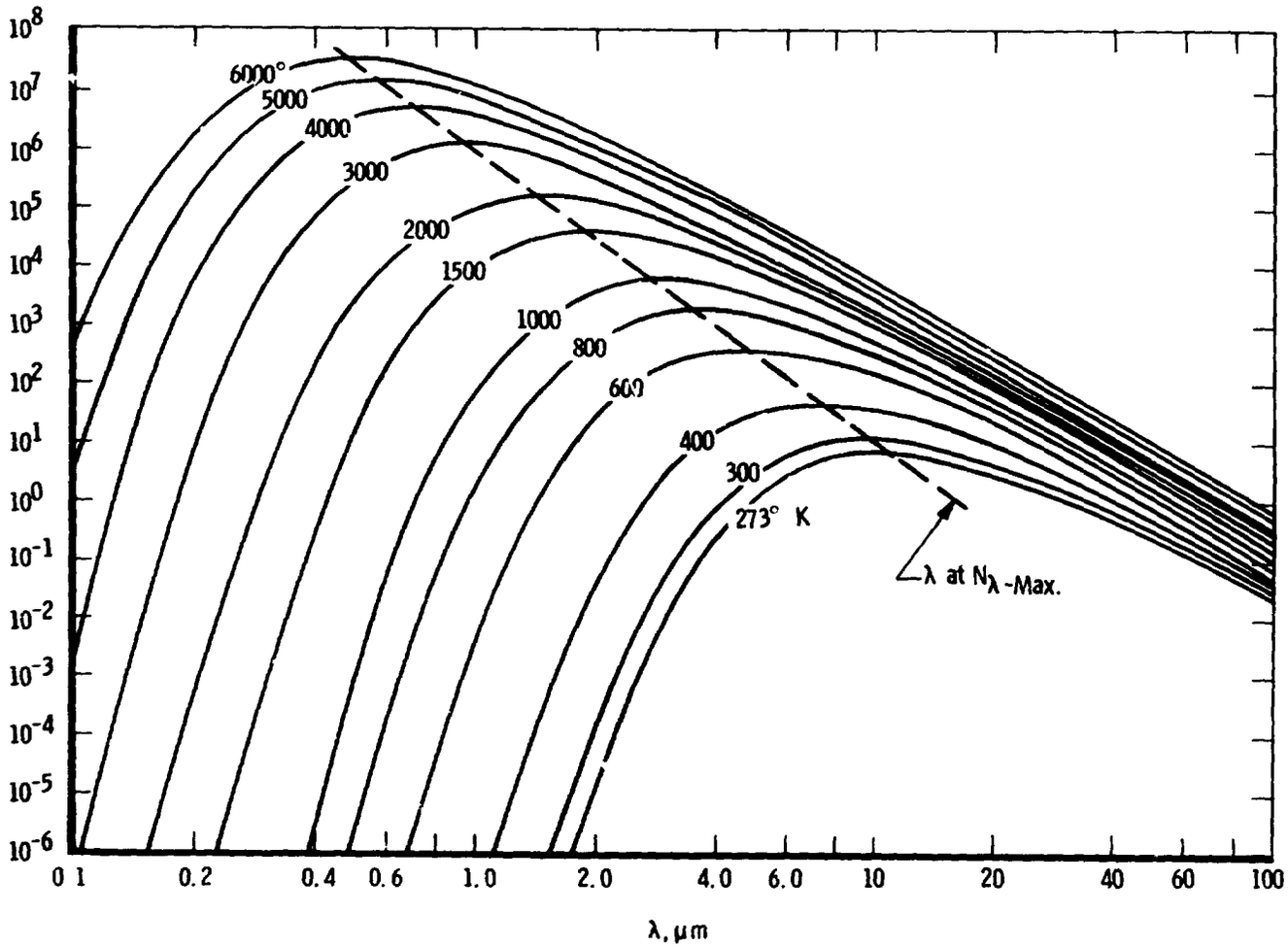

Figure 10. Normal Component of Spectral Radiant Intensity, N_λ, (watt·m^{-2}·sr^{-1}·μm^{-1}) for a Blackbody as a Function of Temperature and Wavelength

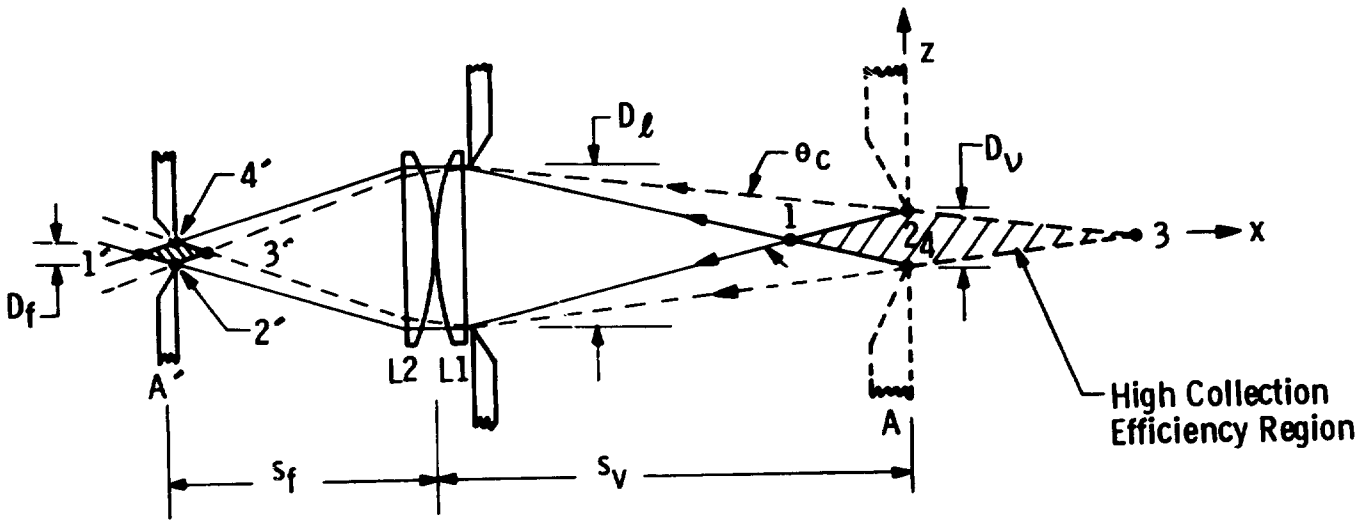

Figure 11. Aperture Lens-Pair Radiation Collection Diagram

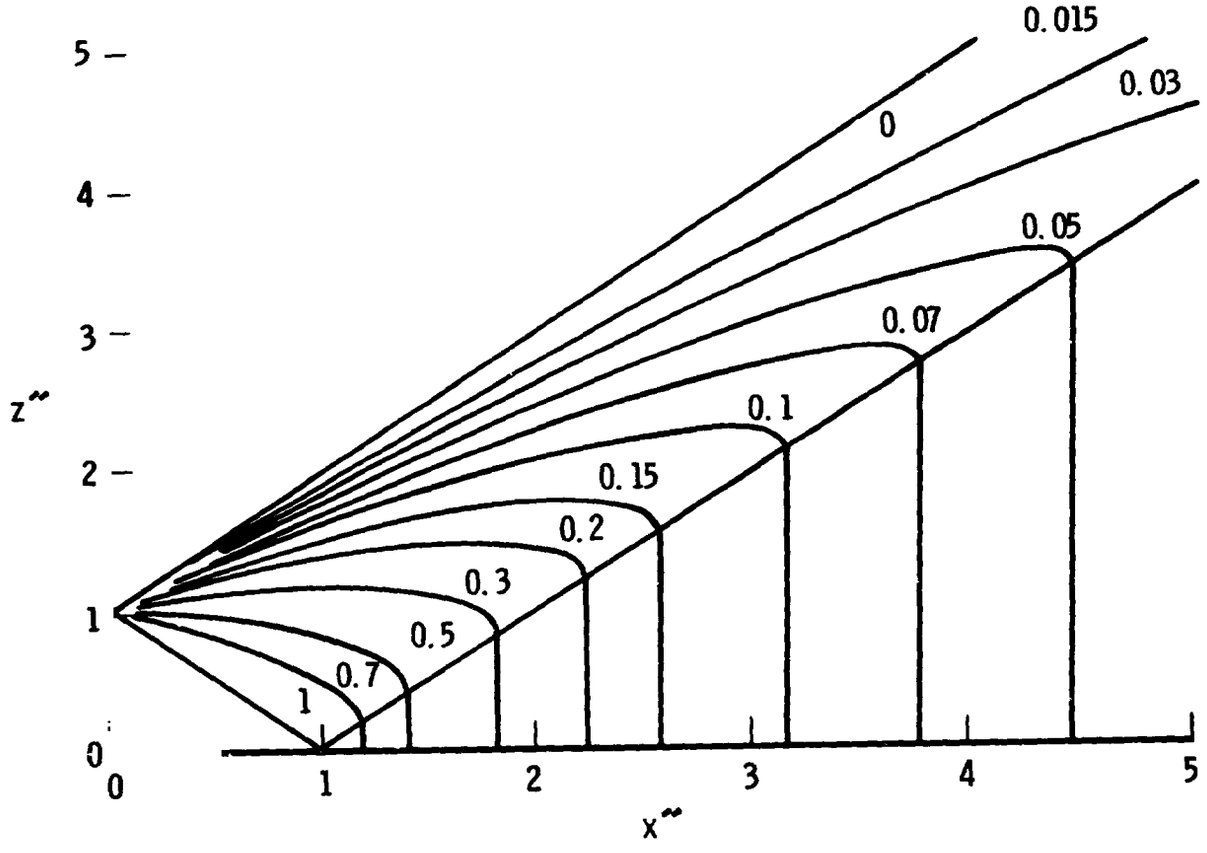

Figure 12. Contour Plot of Relative Radiation Collection Efficiency for the Optical System of Figure 9

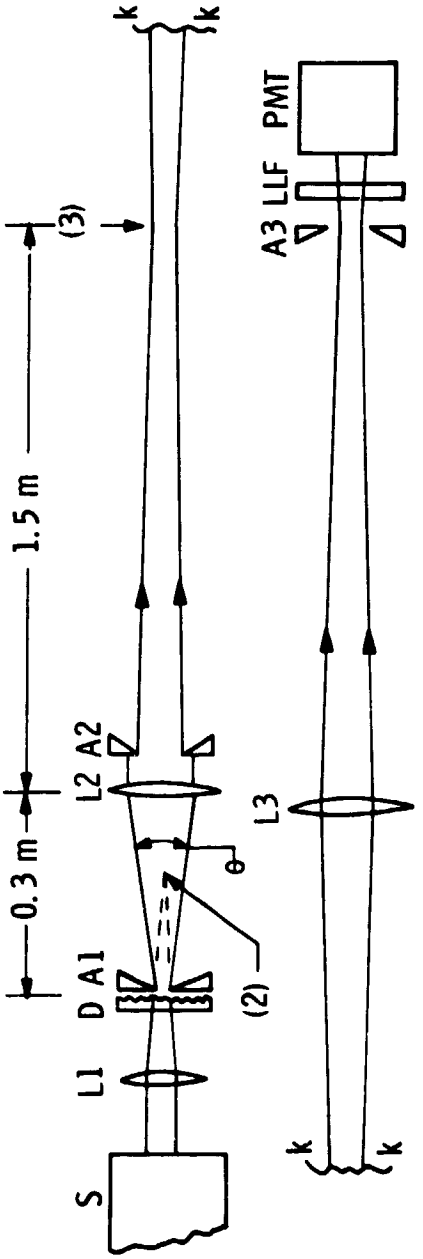

Figure 13. Particle Rate Monitor Optics